https://doi.org/10.5194/acp-2020-474
Preprint. Discussion started: 4 June 2020

Atmospheric Chemistry and Physics Discussions

Optical source apportionment and radiative forcing of light-absorbing carbonaceous aerosol at a tropical marine monsoon climate zone: the importance of ship emissions

Qiyuan Wang[1,2], Huikun Liu[1], Ping Wang[3], Wenting Dai[1], Ting Zhang[1], Youzhi Zhao[3], Jie Tian[1], Wenyan Zhang[1], Yongming Han[1,2], Junji Cao[1,2]

[1]Key Laboratory of Aerosol Chemistry and Physics, State Key Laboratory of Loess and Quaternary Geology, Institute of Earth Environment, Chinese Academy of Sciences, Xi'an 710061, China
[2]CAS Center for Excellence in Quaternary Science and Global Change, Xi'an 710061, China
[3]Hainan Tropical Ocean University, Sanya 572022, China

Correspondence to: Qiyuan Wang (wangqy@ieecas.cn) and Junji Cao (cao@loess.llqg.ac.cn)

Abstract. Source-specific optical properties of light-absorbing carbonaceous (LAC) aerosol are poorly understood owing to its various sources in the atmosphere. Here, a receptor model coupling multi-wavelength absorption with chemical species was utilized to explore the source-specific LAC optical properties at a tropical marine monsoon climate zone. Results showed that biomass burning contributed the largest to LAC absorption on average, but ship emissions became the dominant contributor (44 – 45%) when the air masses originated from the South China Sea. The source-specific absorption Ångström exponent indicates that black carbon (BC) was the dominant LAC aerosol in ship and motor vehicle emissions while there was also brown carbon (BrC) existed in biomass-burning emissions. The source-specific mass absorption cross section (MAC) showed that BC from ship emissions had a stronger light-absorbing capacity than biomass burning and motor vehicle emissions. The BrC MAC derived from biomass burning was smaller than BC MAC and highly depended on wavelengths. Radiative effect assessment indicates a comparable atmospheric forcing and heating capacity of LAC aerosol from biomass burning and ship emissions. Our study provides insights into the optical properties of LAC aerosol from various sources and can improve our understanding of the LAC radiative effects caused by ship emissions.

https://doi.org/10.5194/acp-2020-474
Preprint. Discussion started: 4 June 2020


Atmospheric Chemistry and Physics Discussions

1 Introduction

Carbonaceous aerosol is ubiquitous in the atmosphere and is abundant in $PM_{2.5}$ (particulate matter with an aerodynamic diameter ≤ 2.5 μm) (e.g., 20 – 50% of $PM_{2.5}$ mass) (Putaud et al., 2010; Tao et al., 2017). It has been extensively concerned due to its significant implications for global climate forcing (IPCC, 2013). Among the complex carbonaceous composition, there is a group of substances in relation with light absorption, which is named light-absorbing carbonaceous (LAC) aerosol. The LAC aerosol consists of black carbon (BC) and brown carbon (BrC). BC is a short-lived climate forcer with strong sunlight absorption and has been regarded as the second largest contributor to anthropogenic positive climate forcing after carbon dioxide (Bond et al., 2013). BrC refers to a class of light-absorbing organic compounds with enhanced light absorption towards short wavelengths (e.g., near-ultraviolet region) and, therefore, is a potential contributor to atmospheric heating both on global and regional scales (Laskin et al., 2015).

The optical properties of LAC aerosol are closely related to sources. However, distinguishing source-specific LAC light absorption from a mixture bulk one still remains challenging in the atmosphere. One can use multi-wavelength light absorption data to realize the optical source apportionment based on the Beer-Lambert's Law (e.g., aethalometer model and multi-wavelength absorption analyzer model) (Sandradewi et al., 2008; Massabò et al., 2015). This method can typically explain two different types of sources (e.g., fossil fuel versus biomass burning) that contribute to LAC light absorption, and the results are highly relied on the source-specific absorption Ångström exponent (AAE) used in models. However, owing to the lack of access to obtaining these AAE data, most studies applied empirical values reported in other literatures (e.g., Healy et al., 2017; Küpper et al., 2018; Zheng et al., 2019). This may lead to a large uncertainty to the results, because the source-specific AAEs are site-dependent variables and varies with fuel types and their burning efficiencies (Tian et al., 2019).

In addition, optical source apportionment can also be realized by receptor models (e.g., positive matrix factorization (PMF) and multilinear engine (ME2)). Several studies have utilized a receptor model to identify the sources firstly based on the sole chemical species or mass spectra information, and then a multiple linear regression model is further used to apportion the contribution of each source to the aerosol optical parameters (e.g., Qin et al., 2018; Tian et al., 2020). This method can be called indirect optical

https://doi.org/10.5194/acp-2020-474
Preprint. Discussion started: 4 June 2020


Atmospheric Chemistry and Physics Discussions

source apportionment. In contrast, Forello et al. (2019) coupled chemical species with multi-wavelength absorption in ME2 to directly perform the optical source apportionment. Compared with indirect approach, the additional optical data in receptor model can improve the performance of source apportionment, because each source has its own optical features. Furthermore, it may also avoid some potential uncertainties caused by multiple operations of indirect approach. However, the application of direct optical source apportionment is lack at present.

Alternatively, laboratory study is also an effective way to explore the characteristics of LAC optical properties of a specific source (e.g., vehicle engine exhaust, coal combustion, and biomass burning) (Tian et al., 2019; Xie et al., 2017). However, owing to the complex atmospheric processes experienced by LAC aerosol after it emitted to the atmosphere, the features of LAC optical properties may change significantly. Thus, it is critical to identify the LAC aerosol of different sources in the atmosphere through certain method to obtain their optical properties. Furthermore, as an important part of emissions from transportation sector, to our knowledge, there is no study focusing on the optical properties of ship exhaust-related LAC aerosol in the atmosphere. This hinders our in-depth understanding of the role of ship emissions in climate effects.

In this study, multi-wavelength aerosol light absorption and chemical species were measured in a coastal city of China to investigate the LAC optical properties of ship emissions and other sources. The dataset joining optical and chemically speciated data was used simultaneously in a receptor model to realize the optical source apportionment; then, the source-specific LAC optical properties were determined and characterized; finally, the impacts of radiative forcing induced by LAC aerosol from different sources were evaluated. Our study provides insights into the source-specific LAC optical properties from various sources and will improve our understanding of the radiative effects of LAC aerosol.

2 Methodology

2.1 Sampling site

The sampling site is located in Sanya, a small city (an area of 1921.5 km^2 and a total population of 0.59 million in 2017) at the southernmost tip of Hainan Island in southern China (Fig. S1). Intensive

https://doi.org/10.5194/acp-2020-474
Preprint. Discussion started: 4 June 2020


Atmospheric Chemistry and Physics Discussions

measurements were conducted in spring from 12 April to 14 May 2017 at the rooftop of a teaching building (about 20 m above ground level) at Hainan Tropical Ocean University (18.30° N, 109.52° E). The sampling site is surrounded by an educational and residential area with no obvious pollution source in the vicinity. As a tropical marine monsoon climate zone, the weather of Sanya was warm (temperature = 28 ± 3°C) and wet (relative humidity = 81 ± 12%) during the campaign.

2.2 Online and offline measurements

A Model AE33 aethalometer (Magee Scientific, Berkeley, CA, USA) was used to determine the aerosol light absorption coefficients at multi-wavelengths (Abs(λ), λ is wavelength) with a $PM_{2.5}$ cyclone (SCC 1.829, BGI Inc. USA). The collected particles were desiccated with a Nafion® dryer (MD-700-24S-3; Perma Pure, Inc., Lakewood, NJ, USA) before they measured by AE33 aethalometer. As described previously, seven light emitting diodes (λ = 370, 470, 520, 590, 660, 880, and 950 nm) in AE33 aethalometer are used to irradiate the filter deposition spot to obtain the light attenuation (Drinovec et al., 2015). One of the advantages of AE33 measurement is that it resolves filter loading effect using a dual-spot compensation technique. More details regarding AE33 principle can be found in Drinovec et al. (2015).

A photoacoustic extinctiometer (PAX, Droplet Measurement Technologies, Boulder, CO, USA) was used to directly measure the aerosol light absorption at λ = 532 nm. The PAX adopts an intracavity photoacoustic technique, with a modulated laser beam heating up those sampled particles in an acoustic chamber. The heating generated pressure wave is then detected by a sensitive microphone. Meanwhile, the aerosol light scattering can also be measured with a wide-angle integrating reciprocal nephelometer in a scattering chamber. During the campaign, different concentration gradients of ammonium sulphate and freshly-generated propane soot were used to calibrate the light scattering and absorption measurements, respectively. The calibration procedure is described in detail in Q. Wang et al. (2018a).

$PM_{2.5}$ quartz-fiber filters (QM/A; GE Healthcare, Chicago, IL, USA) were collected during daytime (from 08:00 to 20:00) and nighttime (from 20:00 to 08:00 the next day) using a high-volume air sampler (Tisch Environmental, Inc., USA). Before sampling, the blank quartz-fiber filters were heated in a muffle furnace at 805 °C for 3h to remove the possible impurities. After sampling, the quartz-fiber filters were saved in

https://doi.org/10.5194/acp-2020-474
Preprint. Discussion started: 4 June 2020


Atmospheric Chemistry and Physics Discussions

a freezer at about -20 °C to minimize evaporation of volatile materials before chemical analyses. Field blanks were collected and analysed to eliminate the potential background artifacts.

An energy-dispersive X-ray fluorescence (ED-XRF) spectrometry (Epsilon 5 ED-XRF, PANalytical B.V., Netherlands) was used to determine the inorganic elements, including titanium (Ti), vanadium (V), manganese (Mn), ferrum (Fe), nickel (Ni), copper (Cu), zinc (Zn), and bromine (Br). A detailed description of ED-XRF principle may be found in Xu et al. (2012). A thermal/optical carbon analyzer (Desert Research Institute Model 2001, Atmoslytic Inc., Calabasa, CA, USA) was used to analyse the carbonaceous matter, including organic carbon (OC) and elemental carbon (EC). More detailed analytical procedure has been described elsewhere (Chow et al., 2007). An ion chromatograph (IC, Dionex 600; Dionex Corporation, Sunnyvale, CA, USA) was used to quantify the water-soluble cations (i.e., Na^+, K^+, Mg^{2+}, Ca^{2+}, and NH_4^+) and anions (i.e., Cl^-, NO_3^-, and SO_4^{2-}). A detailed description of this instrument may be found in Zhang et al. (2011). An in-injection port thermal desorption (TD) coupled with an Agilent 7890/5975C gas chromatography/mass spectrometer (GC/MS) (Agilent Technologies, Santa Clara, CA, USA) was used to determine the hopanes. A detailed description of TD-GC/MS operation may be found in Wang et al. (2016).

2.3 Segregation of BC and BrC absorption

The Abs(λ) consists of light absorption caused by LAC aerosol (BC and BrC) and mineral dust (Wang et al., 2013). The LAC absorption ($Abs_{LAC}(\lambda)$) therefore was calculated as follows:

$$Abs_{LAC}(\lambda) = Abs_{BC}(\lambda) + Abs_{BrC}(\lambda) = Abs(\lambda) - Abs_{mineral}(\lambda) \quad (1)$$

where $Abs_{BC}(\lambda)$, $Abs_{BrC}(\lambda)$, and $Abs_{mineral}(\lambda)$ are the light absorption contributed by BC, BrC, and mineral dust at λ = 370, 470, 520, 590, 660, or 880 nm, respectively (in unit of Mm^{-1}). The $Abs_{mineral}(\lambda)$ was retrieved from the optical source apportionment as discussed below. With an assumption of only BC absorbing at λ = 880 nm, the $Abs_{BC}(\lambda)$ at wavelengths of 370, 470, 520, 590, and 660 can be extrapolated as follows:

$$Abs_{BC}(\lambda) = Abs(880) \times \left(\frac{\lambda}{880}\right)^{-AAE_{BC}} \quad (2)$$

where AAE_{BC} represents BC AAE, which was assumed to be 1.1 according to the study of Lack and Langridge (2013). Combining Eqs. (1) and (2) gave the following equation:

https://doi.org/10.5194/acp-2020-474
Preprint. Discussion started: 4 June 2020


Atmospheric Chemistry and Physics Discussions

$$\mathrm{Abs_{BrC}}(\lambda) = \mathrm{Abs}(\lambda) - \mathrm{Abs}(880) \times \left(\frac{\lambda}{880}\right)^{-\mathrm{AAE_{BC}}} - \mathrm{Abs_{mineral}}(\lambda) \quad (3)$$

From the perspective of emission and formation, Abs(λ) can be divided into light absorption contributed by primary emissions ($\mathrm{Abs_{pri}}(\lambda)$) and secondary formation ($\mathrm{Abs_{sec}}(\lambda)$). Thus, the Abs(λ) can be calculated as follows:

$$\mathrm{Abs}(\lambda) = \mathrm{Abs_{pri}}(\lambda) + \mathrm{Abs_{sec}}(\lambda) \quad (4)$$

A BC-tracer method was utilized to separate $\mathrm{Abs_{sec}}(\lambda)$ from $\mathrm{Abs_{pri}}(\lambda)$ (Wang et al., 2019a). Thus, the Eq. (4) can be further developed as follows:

$$\mathrm{Abs_{sec}}(\lambda) = \mathrm{Abs}(\lambda) - \left(\frac{\mathrm{Abs}(\lambda)}{\mathrm{BC}}\right)_{\mathrm{pri}} \times [\mathrm{BC}] \quad (5)$$

where $\left(\frac{\mathrm{Abs}(\lambda)}{\mathrm{BC}}\right)_{\mathrm{pri}}$ describes the ratio of Abs(λ) to BC mass concentration in primary emissions (in unit of $\mathrm{m^2\ g^{-1}}$); and [BC] denotes the mass concentration of BC in the atmosphere (in unit of $\mu\mathrm{g\ m^{-3}}$), which was retrieved from the relationship between Abs(880) measured by AE33 aethalometer and EC mass concentration. The $\left(\frac{\mathrm{Abs}(\lambda)}{\mathrm{BC}}\right)_{\mathrm{pri}}$ ratio was determined with a minimum *R*-squared (MRS) method, which is described in detail in Wang et al. (2019a).

2.4 Estimation of optical parameters

AAE reflects spectral dependence of aerosol light absorption, which can be used as an indicator to distinguish the chemical composition of LAC aerosol. For example, LAC aerosol dominated by BC has an AAE closing to 1.0 while the presence of BrC results in AAE larger than 1.0 (Andreae and Gelencsér, 2006). As described previously, AAE can be retrieved using a power law function as follows (Andreae and Gelencsér, 2006):

$$\mathrm{Abs}(\lambda) = \mathrm{C} \times \lambda^{-\mathrm{AAE}} \quad (6)$$

where C is a constant independent of wavelength.

The mass absorption cross-section (MAC) can be used to reflect aerosol light absorption capacity. The MACs of BC and BrC at different wavelengths ($\mathrm{MAC_{BC}}(\lambda)$ and $\mathrm{MAC_{BrC}}(\lambda)$, respectively) were calculated with $\mathrm{Abs_{BC}}(\lambda)$ and $\mathrm{Abs_{BrC}}(\lambda)$ dividing by the corresponding mass concentrations of BC and OC, respectively:

https://doi.org/10.5194/acp-2020-474
Preprint. Discussion started: 4 June 2020


Atmospheric Chemistry and Physics Discussions

$$\mathrm{MAC_{BC}}(\lambda) = \frac{\mathrm{Abs_{BC}}(\lambda)}{[\mathrm{BC}]} \quad (7)$$

$$\mathrm{MAC_{BrC}}(\lambda) = \frac{\mathrm{Abs_{BrC}}(\lambda)}{[\mathrm{OC}]} \quad (8)$$

2.5 Receptor model source apportionment

Here the PMF version 5.0 (PMF5.0) was applied to determine the contributions of various sources to Abs(λ). The principle of PMF has been described elsewhere (Paatero and Tapper, 1994). Briefly, PMF decomposes the initial dataset into a factor contribution matrix $\mathrm{G_{ik}}$ ($i \times k$ dimensions) and a factor profile matrix $\mathrm{F_{kj}}$ ($k \times j$ dimensions), and then iteratively minimizes the object function Q:

$$\mathrm{X_{ij}} = \sum_{k=1}^{p} \mathrm{G_{ik}F_{kj}} + \mathrm{E_{ij}} \quad (9)$$

$$Q = \sum_{i=1}^{m} \sum_{j=1}^{n} \left(\frac{\mathrm{E_{ij}}}{\sigma_{ij}}\right)^2 \quad (10)$$

where $\mathrm{X_{ij}}$ is the value of jth species in ith sample; $\mathrm{E_{ij}}$ describes the model residual; and σ_{ij} represents uncertainty.

2.6 Cluster analysis of air-mass trajectories

Cluster analysis of three-day backward air-mass trajectories was used to investigate the impacts of transport pathways on Abs(λ). The backward trajectories were calculated hourly for arrival height of 500 m above ground level using the Hybrid Single-Particle Lagrangian Integrated Trajectory model (Draxler and Rolph, 2003). The cluster analysis was based on the angle-based distance statistics method, which is defined as follows (Q. Wang et al., 2018a):

$$\mathrm{d_{12}} = \frac{1}{n} \sum_{i=1}^{n} \cos^{-1}\left(0.5 \times \frac{\mathrm{A_i + B_i - C_i}}{\sqrt{\mathrm{A_i B_i}}}\right) \quad (11)$$

$$\mathrm{A_i} = (\mathrm{X_1(i) - X_0})^2 + (\mathrm{Y_1(i) - Y_0})^2 \quad (12)$$

$$\mathrm{B_i} = (\mathrm{X_2(i) - X_0})^2 + (\mathrm{Y_2(i) - Y_0})^2 \quad (13)$$

$$\mathrm{C_i} = (\mathrm{X_2(i) - X_1(i)})^2 + (\mathrm{Y_2(i) - Y_1(i)})^2 \quad (14)$$

where $\mathrm{d_{12}}$ denotes the mean angle that varies from 0 to π between two backward trajectories; n is the total number of end points of a trajectory; $\mathrm{X_0}$ and $\mathrm{Y_0}$ describe the position of the receptor site (e.g., Sanya for

https://doi.org/10.5194/acp-2020-474
Preprint. Discussion started: 4 June 2020


Atmospheric Chemistry and Physics Discussions

the current case); and X_1 (Y_1) and X_2 (Y_2) represent the backward trajectories 1 and 2, respectively. The calculations were performed by a GIS-based TrajStat software developed by Wang et al. (2009).

2.7 Estimations of radiative forcing and heating rate

The LAC direct radiative forcing (DRF) was estimated by the Santa Barbara DISORT (Discrete Ordinate Radiative Transfer) Atmospheric Radiative Transfer (SBDART) model in the shortwave spectral region of 0.25 – 4.0 μm. The principle of SBDART model is described in detail in Ricchiazzi et al. (1998). The measured mass concentrations of OC, EC, and water-soluble ions as well as the estimated dust loading (=[Fe]/0.035) during the daytime were used in the Optical Properties of Aerosol and Cloud (OPAC) model to estimate the single scattering albedo, aerosol optical depth, and asymmetric parameter. These are essential input parameters in SBDART model. More detailed description of the software package OPAC can be found in Hess et al. (1998). The light absorption, light scattering, and single scattering albedo measured by PAX were used to constrain the performance of OPAC, and small differences were found between modelled and measured values (Fig. S2). The DRFs induced by LAC aerosol of different sources at the Earth's surface and the top of the atmosphere were calculated by difference in the net flux with and without source-specific LAC aerosol under cloud-free conditions.

Further, the atmospheric heating rate ($\frac{\partial T}{\partial t}$, in unit of K d^{-1}) caused by LAC aerosol was estimated using the first law of thermodynamics and hydrostatic equilibrium as follows (Liou, 2002):

$$\frac{\partial T}{\partial t} = \frac{g}{C_p} \times \frac{\Delta F}{\Delta P} \quad (15)$$

where $\frac{g}{C_p}$ is the lapse rate, of which g represents the acceleration due to gravity while C_p describes the specific heat capacity of air at a constant pressure (1006 J kg^{-1} K^{-1}); ΔF is the atmospheric forcing contributed by LAC aerosol; and ΔP represents the atmospheric pressure difference (300 hPa).

https://doi.org/10.5194/acp-2020-474
Preprint. Discussion started: 4 June 2020


Atmospheric Chemistry and Physics Discussions

3 Results and discussion

3.1 Overview of Abs(λ)

Owing to the matrix scattering effect, AE33 absorption was first corrected using the PAX measurement, and a strong correlation ($r = 0.96$, $p < 0.01$) was found between them (Fig. S3). The slope of 2.3 was regard as the correction factor, which is comparable to values of 2.0 – 2.6 reported in previous studies using similar method (Qin et al., 2018; Tasoglou et al., 2017; Wang et al., 2019b). After correction, the average Abs(λ) were 15.7 ± 5.3, 11.4 ± 3.7, 9.7 ± 3.0, 8.3 ± 2.6, 7.0 ± 2.2, and 4.9 ± 1.5 Mm^{-1} at 370, 470, 520, 590, 660, and 880 nm during the campaign, respectively (Fig. S4). However, it should be noted that such single-wavelength calibration may overestimate Abs(λ) at long wavelengths (i.e., λ = 590, 660, 880 nm) while underestimate at short wavelengths (i.e., λ = 370 and 470 nm) owing to the wavelength dependence of correction factor (Kim et al., 2019). Compared with previous studies (J. Wang et al., 2018; Liakakou et al., 2020; Zanatta et al., 2016; Zhu et al., 2017), the Abs(λ) here is lower than those from urban areas in China and Europe but comparable to some rural and remote areas, where the anthropogenic activities are not intensive. This suggests a relatively small LAC burden in the atmosphere at Sanya during the campaign.

From the perspective of LAC components, the $Abs_{BC}(\lambda)$ contributed more than 77% to Abs(λ), whereas the contribution of $Abs_{BrC}(\lambda)$ was less than 17% (Fig. S4). This is consistent with previous studies showing that BC is a stronger light absorber than BrC from near-ultraviolet to near-infrared wavelengths in the atmosphere (Massabò et al., 2015; Liakakou et al., 2020). However, laboratory studies reported that $Abs_{BrC}(\lambda)$ can exceed $Abs_{BC}(\lambda)$ at short wavelengths in fresh biomass-burning smokes, especially for smoldering phase (Tian et al., 2019; Chow et al., 2018). As shown in Fig. S4, the fraction of $Abs_{BC}(\lambda)$ enhanced as the wavelength increased, but the fraction of $Abs_{BrC}(\lambda)$ showed an inverse trend, with a dramatical dropping from 17% at 370 nm to 3% at 660 nm, suggesting a stronger light-absorbing capacity for BrC at short wavelength than long one. From relationship between Abs(λ) and carbonaceous composition (Fig. S5), $Abs_{BC}(\lambda)$ correlated well ($r = 0.93$, $p < 0.01$) with EC mass concentration while a weak but significant correlation ($r = 0.27 – 0.42$, $p < 0.05$) was found between $Abs_{BrC}(\lambda)$ and OC mass concentration. The results further conform that BC was the dominant light-absorbing material in LAC

https://doi.org/10.5194/acp-2020-474
Preprint. Discussion started: 4 June 2020


Atmospheric Chemistry and Physics Discussions

aerosol while OC comprised more non-light-absorbing carbon components relative to the light-absorbing one.

3.2 Source apportionment of Abs(λ)

To quantify the contributions of various sources to Abs(λ), the chemical species and $Abs_{pri}(\lambda)$ were used simultaneously as input parameters in PMF5.0 model. The selected chemical species included carbonaceous matter (i.e., OC and EC), water-soluble cations (i.e., Na^+, K^+, and Ca^{2+}), elements (i.e., Ti, V, Mn, Fe, Ni, Cu, Zn, Br), and hopanes, and their mass concentrations are summarized in Table S1. Based on Eq. (5), the $Abs_{sec}(\lambda)$ explained less than 5% of Abs(λ) (Table S2), suggesting a negligible impact of secondary formation during the campaign. Thus, the uncertainty caused by the only use of $Abs_{pri}(\lambda)$ in model could be neglected in the absence of effective way to identify the sources of light absorption contributed by secondary organic aerosol. After multiple runs of PMF5.0 model, four sources of light absorption were identified, including ship emissions, motor vehicle emissions, biomass burning, and mineral dust (Fig. 1a). The modeled $Abs_{pri}(\lambda)$ at different wavelengths showed strong correlations ($r = 0.82 – 0.89$, $p < 0.01$) with those measured Abs(λ) (Fig. S6). The slopes of 0.92 – 0.98 were consistent with the absorption fractions of $Abs_{pri}(\lambda)$ estimated by the BC-tracer method combined with the MRS approach (Table S2). The scaled residuals for each species varied between -3 and +3. These results suggest a good performance of PMF5.0 model in performing the optical source apportionment.

As shown in Fig. 1a, the first source factor was characterized by large loadings of V, Ni, and hopanes as well as moderate contributions of OC, EC, Na^+, K^+, Cu, and $Abs_{pri}(\lambda)$. V and Ni are associated with oil fuel combustion (Moreno et al., 2010), and their ratio (V/Ni) can be used to further identify the ship engine emissions, which has a typical range of 2.5 – 4.0 (Cesari et al., 2014). The estimated V/Ni ratio was 3.4 in this source factor, consistent with the feature of ship engine emissions. Because the hydrocarbon is the major component of ship engine oil fuel, the hopanes, OC, and EC can be produced as byproducts in the combustion process. This source factor was therefore assigned to ship emissions. The second source factor was featured with large loadings of Cu, Zn, and Br as well as moderate contributions of hopanes, EC, Ti, and $Abs_{pri}(\lambda)$. Previous studies have confirmed that hopanes, Br, and EC typically consist in vehicle exhaust particles (Huang et al., 1994; Sheesley et al., 2009), and Zn and

https://doi.org/10.5194/acp-2020-474
Preprint. Discussion started: 4 June 2020


Atmospheric Chemistry and Physics Discussions

Cu are associated with the lubricant and metal brake wear (Lin et al., 2015). Thus, this source factor was allocated to motor vehicle emissions. The third source factor was dominated by high contributions of K^+, OC, EC, and $Abs_{pri}(\lambda)$, which was an obvious feature of biomass burning (Forello et al., 2019). The fourth source factor was characterized by large loadings of several crustal materials, such as Ca^{2+}, Ti, Fe, and Mn, and, therefore, it was identified as mineral dust.

As shown in Fig. 1b, biomass burning was the largest contributor on average, constituting 32 – 44% of $Abs_{pri}(\lambda)$. As a coastal city with heavy maritime traffic (e.g., the cargo handling capacity was larger than 5.8 million tons in 2017 at Sanya port, http://tjj.sanya.gov.cn/tjjsite/2019nnj/tjnj.shtml, in Chinese), ship emissions also contributed significantly to $Abs_{pri}(\lambda)$ (30 – 39%). The contribution of motor vehicle emissions (17 – 24% of $Abs_{pri}(\lambda)$) was much lower than biomass burning and ship emissions. Moreover, the mineral dust explained less than 10% of $Abs_{pri}(\lambda)$, consistent with its role of minor contribution in the atmosphere (Yang et al., 2009; Zhao et al., 2019). This small absorption fraction may be mainly attributed to the low content of light-absorbing iron oxides in the atmosphere. As shown in Fig. 1c, the $Abs_{pri}(\lambda)$ of different sources all decreased with the increased wavelength, but their relative contributions exhibited distinct trends. The absorption fractions of ship and motor vehicle emissions enhanced as the wavelength increased while a reverse trend was observed for biomass burning. This discrepancy can be explained by the large amount of BrC existed in biomass-burning emissions, which can result in more light absorption at short wavelengths relative to long ones (see Fig. S4).

To investigate the impacts of regional transport on $Abs_{pri}(\lambda)$, three-day backward trajectories were grouped into four cluster-mean trajectories (Fig. 2). The air masses associated with Cluster #1 derived from the South China Sea. With a high vessel traffic density over the South China Sea, ship emissions are the largest contributor, constituting 44 – 45% of $Abs_{pri}(\lambda)$. This cluster comprised 44% of total trajectories, suggesting that Sanya was often subjected to the influences of ship exhaust-related LAC aerosol transported from the South China Sea. Cluster #2 originated from the South China Sea near the Indochina Peninsula, which contained 35% of total trajectories. Ship emissions were also vital in this cluster, accounting for 34 – 37% of $Abs_{pri}(\lambda)$. However, owing to the large burden of biomass-burning-related carbonaceous aerosol in Southeast Asia (Li et al., 2017), biomass burning contributed more to $Abs_{pri}(\lambda)$ (36 – 43%) than ship emissions. This can be further confirmed by numerous fire counts observed

https://doi.org/10.5194/acp-2020-474
Preprint. Discussion started: 4 June 2020


Atmospheric Chemistry and Physics Discussions

in Vietnam (Fig. 2), which is near the origination area of Cluster #2. Small number of air masses were grouped into Cluster #3 and Cluster #4, comprising only 6% and 15% of total trajectories, respectively. Cluster #3 derived from southern Burma and passed over Thailand, Laos, and Vietnam, where there were intensive biomass-burning activities (Fig. 2). Cluster #4 had the longest cluster-mean trajectory which originated and passed through the coastal areas of southeastern China. For these two clusters, biomass burning was the dominant contributor to $Abs_{pri}(\lambda)$, with 62 – 69% for Cluster #3 and 56 – 64% for Cluster #4.

3.3 Source-dependent optical properties of LAC aerosol

Retrieved from a power law function, the average LAC AAE (1.4) was greater than unity during the campaign (Fig. 3), indicating the presence of both BC and BrC in the atmosphere. As shown in Fig. 3, the estimated AAE of motor vehicle emissions ($AAE_{vehicle}$) was 1.0, closing to values (0.9 – 1.1) obtained from ambient observations using radiocarbon method and the vehicle exhaust-related source experiments (Sandradewi et al., 2008; Chow et al., 2018; Zotter et al., 2017). This narrow range of $AAE_{vehicle}$ among studies suggests that the spectral dependence of vehicle exhaust-related LAC absorption is less affected by atmospheric processes. The AAE of ship emissions (AAE_{ship} = 1.1) showed a similarity with $AAE_{vehicle}$. These low spectral dependences of light absorption indicate that BC was the dominant contributor to LAC aerosol in ship and motor vehicle emissions. Compared to marine engine emissions, the AAE_{ship} in this study is consistent with values derived from marine gas oil and diesel fuel emissions (1.0 ± 0.1) but lower than heavy fuel oil exhaust (1.7 ± 0.2) (Corbin et al., 2018). This comparison reflects that Sanya may be more likely influenced by those ships using distillate fuels relative to heavy fuel oil.

The AAE of biomass burning ($AAE_{biomass}$ = 1.8) was larger than those from ship and motor vehicle emissions, implying the presence of BrC in biomass-burning-related LAC aerosol in addition to BC. This is consistent with previous studies showing that BrC is mainly derived from biomass burning rather than fossil fuel in the atmosphere (Laskin et al., 2015). Although chamber studies have shown that AAEs of fresh biomass-burning smokes vary largely (e.g., 1.64 – 3.25) depending on the types of biomass and their burning efficiencies (Tian et al., 2019), the $AAE_{biomass}$ in this study is close to those (1.7 – 1.9) in the atmosphere constrained by radiocarbon method (Sandradewi et al., 2008; Zotter et al., 2017). As our

https://doi.org/10.5194/acp-2020-474
Preprint. Discussion started: 4 June 2020


Atmospheric Chemistry and Physics Discussions

approach can retrieve the source-specific AAEs in the atmosphere, it can improve the performance of those optical source apportionment models that bases on sole optical data.

Owing to the dominance of BC in ship and motor vehicle emissions, only $MAC_{BC}(\lambda)$ was estimated for these two sources. Based on the results of optical source apportionment, the estimated $MAC_{BC}(\lambda)$ of motor vehicle emissions ($MAC_{BC,vehicle}(\lambda)$) were close to values of uncoated BC particles at different wavelengths (Fig. 4). This indicates that vehicle exhaust-related BC particles were mainly associated with local emissions and experienced minor atmospheric aging processes. By contrast, the $MAC_{BC}(\lambda)$ of ship emissions ($MAC_{BC,ship}(\lambda)$) was 1.4 – 1.6 times larger than uncoated one (Fig. 4), implying that ship exhaust-related BC particles were subject to substantial aging during their transport from ocean. It is unexpected that our $MAC_{BC,ship}(\lambda)$ is similar to the value of marine engine emissions (7.8 $m^2\ g^{-1}$ at 780 nm, extrapolated to the same wavelengths of this study by assuming an $AAE_{BC} = 1.1$) (Corbin et al., 2018), because freshly emitted fossil fuel BC particles tend to be externally-mixed with other substances and become internally-mixed ones after aging (Xing et al., 2020). Actually, the authors of that study also recognize that more work is needed to clarify their ambiguous large $MAC_{BC}(\lambda)$ of marine engine emissions.

As biomass-burning-related LAC aerosol comprised both BC and BrC, the $MAC_{BC}(\lambda)$ and $MAC_{BrC}(\lambda)$ were retrieved based on the results of optical source apportionment (Fig. 4). The $MAC_{BC}(\lambda)$ of biomass burning ($MAC_{BC,biomass}(\lambda)$) was larger than $MAC_{BC,vehicle}(\lambda)$, consistent with previous studies showing a stronger BC light absorption capacity for biomass burning relative to motor vehicle emissions (Qiu et al., 2014; Q. Wang et al., 2018b). Compared with ship emissions, the $MAC_{BC,biomass}(\lambda)$ was smaller than $MAC_{BC,ship}(\lambda)$, suggesting a stronger light-absorbing ability for ship exhaust-related BC particles. A broader implication is that the impacts of ship emission-related BC on climate should be paid more attention owing to the striking increase in shipping activities globally.

The $MAC_{BrC}(\lambda)$ of biomass burning ($MAC_{BrC,biomass}(\lambda)$) was highly wavelength dependent, with 1.7 $m^2\ g^{-1}$ at 370 nm but dropping to near zero (0.04 $m^2\ g^{-1}$) at 660 nm (Fig. 4). The $MAC_{BrC,biomass}(\lambda)$ was several times to two orders of magnitude lower than $MAC_{BC}(\lambda)$ of different sources, suggesting an absolute stronger light absorber for BC relative to BrC. The $MAC_{BrC}(\lambda)$ here is in the range reported by previous investigations though difference was found among studies (Wang et al., 2019b; Cho et al., 2019). This

https://doi.org/10.5194/acp-2020-474
Preprint. Discussion started: 4 June 2020


Atmospheric Chemistry and Physics Discussions

discrepancy of $MAC_{BrC}(\lambda)$ is partially related to biomass types and their burning efficiencies as well as following aging processes of BrC in the atmosphere. In addition, the use of different BrC substitutes (e.g., OC, organic aerosol, or water-soluble organic carbon) is also a cause affecting $MAC_{BrC}(\lambda)$ calculation. Compared with previous laboratory studies, our $MAC_{BrC,biomass}(\lambda)$ is smaller than those from fresh biomass-burning smokes (Zhong and Jang, 2014; Pandey et al., 2016). As photobleaching is an effective way to turn BrC into a transparent organic substance (Laskin et al., 2015), the smaller atmospheric $MAC_{BrC,biomass}(\lambda)$ here may be attributed to the elimination of organic chromophores induced by bright sunlight at Sanya.

The MAC links LAC mass to its light absorption, which is an important parameter in climate models to evaluate global or regional LAC radiative effects. Because identifying source-specific MACs still remains challenging in the atmosphere, an equal MAC of different sources is often assumed in climate models (Bond et al., 2013). However, this assumption could cause a large uncertainty owing to the distinct MACs for various sources (e.g., $MAC_{BC,ship}(\lambda) > MAC_{BC,biomass}(\lambda) > MAC_{BC,vehicle}(\lambda)$ in this study). The chemical composition-based optical source apportionment approach may provide a potential solution to resolve this issue, although more source-specific MACs in different areas and seasons are needed in the future study to gauge the accuracy of climate models. Moreover, this approach also can minimize the uncertainties of BC source apportionment using the aethalometer model due to the assumption of equal AAE and MAC of different sources.

3.4 Impacts of LAC aerosol on radiative forcing

Fig. 5 shows the source-specific LAC DRF during the campaign. The LAC DRF varied from -5.5 to -1.6 W m^{-2} at the Earth's surface, with an average cooling effect of -3.2 ± 1.0 W m^{-2}. In contrast, the LAC aerosol produced a warm effect of +1.5 ± 0.5 W m^{-2} at the top of the atmosphere with a range of +0.8 to +2.8 W m^{-2}, suggesting a net energy gain. The presence of LAC aerosol enhanced aerosol forcing at the top of the atmosphere by 62% compared to the result with light scattering aerosol only. The difference between LAC DRF at the top of the atmosphere and the Earth's surface gave the atmospheric forcing (a net atmospheric absorption) of +4.7 ± 1.5 W m^{-2}, which can generate a heating rate of 0.13 ± 0.04 K day^{-1}.

https://doi.org/10.5194/acp-2020-474
Preprint. Discussion started: 4 June 2020


Atmospheric Chemistry and Physics Discussions

From the perspective of LAC absorption sources, biomass burning was the largest contributor to LAC DRF, which were -1.5 ± 0.5 and +0.7 ± 0.2 W m^{-2} at the Earth's surface and the top of the atmosphere, respectively. Although the biomass-burning BrC contributed less to LAC DRF than that produced by BC from the same source, the presence of BrC strengthened the biomass-burning LAC forcing by 21% relative to the result with BC only, suggesting a substantial radiative effect from BrC aerosol. The LAC DRF were -1.1 ± 0.4 and +0.5 ± 0.2 W m^{-2} for ship emissions and -0.6 ± 0.2 and +0.3 ± 0.1 W m^{-2} for motor vehicle emissions at the Earth's surface and the top of the atmosphere, respectively. The LAC DRF contributed by ship and motor vehicle emissions was mainly caused by BC aerosol. Although larger BC atmospheric forcing was found for biomass burning, the ship emissions showed an equivalent capacity of radiative forcing production (0.5 (W m^{-2}) (μg m^{-3})$^{-1}$) from per unit BC mass concentration generating atmospheric forcing. By contrast, motor vehicle emissions had a smaller value of 0.3 (W m^{-2}) (μg m^{-3})$^{-1}$. Furthermore, the atmospheric heating rate of LAC aerosol was similar for biomass burning (0.06 ± 0.02 K day^{-1}) and ship emissions (0.05 ± 0.01 K day^{-1}), larger than that produced by motor vehicle emissions (0.03 ± 0.01 K day^{-1}), further indicating the importance of ship exhaust LAC aerosol in atmospheric heating effect.

4 Conclusions

In this study, we explored the optical properties and radiative forcing of light-absorbing carbonaceous (LAC) aerosol in Sanya at a tropical marine monsoon climate zone of China. During the campaign, the light absorption caused by primary emissions ($Abs_{pri}(\lambda)$) was the dominant contributor to LAC absorption ($Abs_{LAC}(\lambda)$) while minor contribution was found for secondary processes. From the perspective of LAC composition, black carbon (BC) aerosol (> 77%) contributed more to $Abs_{LAC}(\lambda)$ than brown carbon (BrC) (< 17%). Coupling chemical species with multi-wavelength absorption in a positive matrix factorization model, we obtained that biomass burning contributed the highest to $Abs_{pri}(\lambda)$ (32 – 44%), followed by ship (30 – 39%) and motor vehicle emissions (17 – 24%), with the smallest for mineral dust (< 10%). Based on the results of cluster analysis of three-day backward trajectories, ship emissions became the largest contributor to $Abs_{pri}(\lambda)$ when the air-masses originated from the South China Sea, whereas biomass burning dominated in other directions.

https://doi.org/10.5194/acp-2020-474
Preprint. Discussion started: 4 June 2020


Atmospheric Chemistry and Physics Discussions

The source-specific absorption Ångström exponent (AAE) showed a similarity between ship and motor vehicle emissions (1.1 versus 1.0). The low spectral dependence of light absorption indicates that LAC aerosol was dominated by BC in ship and motor vehicle emissions. By contrast, a large AAE of 1.8 was found for biomass burning, indicating the presence of both BC and BrC. The source-specific mass absorption cross section (MAC) showed that BC particles from ship emissions had the strongest light-absorbing capacity, followed by biomass burning and motor vehicle emissions. Compared with BC MAC, the BrC MAC of biomass burning was smaller, with a value of 1.7 m^2 g^{-1} at 370 nm but dropping to 0.04 m^2 g^{-1} at 660 nm. The radiative transfer model shows that the atmospheric forcing caused by LAC was +4.7 ± 1.5 W m^{-2} during the campaign, which corresponds to a heating rate of 0.13 ± 0.04 K day^{-1}. The presence of BrC strengthened the biomass-burning LAC forcing by 21% relative to the result with BC only. The ship emissions showed an equivalent capacity of radiative forcing production (0.5 (W m^{-2}) (μg m^{-3})$^{-1}$) from per unit BC mass concentration generating atmospheric forcing. By contrast, motor vehicle emissions had a smaller value of 0.3 (W m^{-2}) (μg m^{-3})$^{-1}$.

Data availability. All data described in this study are available upon request from the corresponding authors.

Supplement. The supplement related to this article is available online.

Author contributions. QW, JC, and YH designed the campaign. PW and YZ provided the observation site and assisted with field sampling and measurements. WD and TZ conducted the chemical analyses. HL ran the PMF5.0 and SBDART model. JT performed the cluster analysis of air-mass trajectories. WZ provided the ArcGIS maps. QW conducted the data analysis and wrote the article with input from all co-authors.

Competing interests. The authors declare that they have no conflict of interest.

https://doi.org/10.5194/acp-2020-474
Preprint. Discussion started: 4 June 2020

Atmospheric Chemistry and Physics Discussions

Acknowledgments. This work was supported by the Strategic Priority Research Program of Chinese Academy of Sciences (XDB40030200), the Youth Innovation Promotion Association of the Chinese Academy of Sciences (2019402), the Hainan Natural Science Foundation High-level Talent Project (2019RC243), and the Science and Technology Cooperation Project of Sanya (2018YD14 and 2012YD38).

References

Andreae, M. O., and Gelencsér, A.: Black carbon or brown carbon? The nature of light-absorbing carbonaceous aerosols, Atmos. Chem. Phys., 6, 3131-3148, https://doi.org/10.5194/acp-6-3131-2006, 2006.

Bond, T. C., Doherty, S. J., Fahey, D. W., Forster, P. M., Berntsen, T., DeAngelo, B. J., Flanner, M. G., Ghan, S., Kärcher, B., Koch, D., Kinne, S., Kondo, Y., Quinn, P. K., Sarofim, M. C., Schultz, M. G., Schulz, M., Venkataraman, C., Zhang, H., Zhang, S., Bellouin, N., Guttikunda, S. K., Hopke, P. K., Jacobson, M. Z., Kaiser, J. W., Klimont, Z., Lohmann, U., Schwarz, J. P., Shindell, D., Storelvmo, T., Warren, S. G., and Zender, C. S.: Bounding the role of black carbon in the climate system: A scientific assessment, J. Geophys. Res.-Atmos., 118, 5380-5552, https://doi.org/10.1002/jgrd.50171, 2013.

Cesari, D., Genga, A., Ielpo, P., Siciliano, M., Mascolo, G., Grasso, F. M., and Contini, D.: Source apportionment of $PM_{2.5}$ in the harbour–industrial area of Brindisi (Italy): Identification and estimation of the contribution of in-port ship emissions, Sci. Total Environ., 497-498, 392-400, https://doi.org/10.1016/j.scitotenv.2014.08.007, 2014.

Cho, C., Kim, S.-W., Lee, M., Lim, S., Fang, W., Gustafsson, Ö., Andersson, A., Park, R. J., and Sheridan, P. J.: Observation-based estimates of the mass absorption cross-section of black and brown carbon and their contribution to aerosol light absorption in East Asia, Atmos. Environ., 212, 65-74, https://doi.org/10.1016/j.atmosenv.2019.05.024, 2019.

Chow, J. C., Watson, J. G., Chen, L. W. A., Chang, M. C. O., Robinson, N. F., Trimble, D., and Kohl, S.: The IMPROVE_A temperature protocol for thermal/optical carbon analysis: Maintaining

https://doi.org/10.5194/acp-2020-474
Preprint. Discussion started: 4 June 2020


Atmospheric Chemistry and Physics Discussions

consistency with a long-term database, J. Air Waste Manage. Assoc., 57, 1014-1023, https://doi.org/10.3155/1047-3289.57.9.1014, 2007.

Chow, J. C., Watson, J. G., Green, M. C., Wang, X., Chen, L. W. A., Trimble, D. L., Cropper, P. M., Kohl, S. D., and Gronstal, S. B.: Separation of brown carbon from black carbon for IMPROVE and Chemical Speciation Network $PM_{2.5}$ samples, J. Air Waste Manage. Assoc., 68, 494-510, https://doi.org/10.1080/10962247.2018.1426653, 2018.

Corbin, J. C., Pieber, S. M., Czech, H., Zanatta, M., Jakobi, G., Massabò, D., Orasche, J., El Haddad, I., Mensah, A. A., Stengel, B., Drinovec, L., Mocnik, G., Zimmermann, R., Prévôt, A. S. H., and Gysel, M.: Brown and black carbon emitted by a marine engine operated on heavy fuel oil and distillate fuels: Optical properties, size distributions, and emission factors, J. Geophys. Res.-Atmos., 123, 6175-6195, https://doi.org/10.1029/2017JD027818, 2018.

Draxler, R. R., and Rolph, G. D.: HYSPLIT (HYbrid Single-Particle Lagrangian Integrated Trajectory), Silver Spring, MD, Model access via NOAA ARL READY Website: http://www.arl.noaa.gov/ready/hysplit4.htmlNOAAAirResourcesLaboratory (last access: November 2019), 2003.

Drinovec, L., Močnik, G., Zotter, P., Prévôt, A. S. H., Ruckstuhl, C., Coz, E., Rupakheti, M., Sciare, J., Müller, T., Wiedensohler, A., and Hansen, A. D. A.: The "dual-spot" Aethalometer: an improved measurement of aerosol black carbon with real-time loading compensation, Atmos. Meas. Tech., 8, 1965-1979, https://doi.org/10.5194/amt-8-1965-2015, 2015.

Forello, A. C., Bernardoni, V., Calzolai, G., Lucarelli, F., Massabò, D., Nava, S., Pileci, R. E., Prati, P., Valentini, S., Valli, G., and Vecchi, R.: Exploiting multi-wavelength aerosol absorption coefficients in a multi-time resolution source apportionment study to retrieve source-dependent absorption parameters, Atmos. Chem. Phys., 19, 11235-11252, https://doi.org/10.5194/acp-19-11235-2019, 2019.

Healy, R. M., Sofowote, U., Su, Y., Debosz, J., Noble, M., Jeong, C. H., Wang, J. M., Hilker, N., Evans, G. J., Doerksen, G., Jones, K., and Munoz, A.: Ambient measurements and source apportionment of fossil fuel and biomass burning black carbon in Ontario, Atmos. Environ., 161, 34-47, https://doi.org/10.1016/j.atmosenv.2017.04.034, 2017.

https://doi.org/10.5194/acp-2020-474
Preprint. Discussion started: 4 June 2020


Atmospheric Chemistry and Physics Discussions

Hess, M., Koepke, P., and Schult, I.: Optical Properties of Aerosols and Clouds: The Software Package OPAC, Bull. Amer. Meteorol. Soc., 79, 831-844, https://doi.org/10.1175/1520-0477(1998)079<0831:OPOAAC>2.0.CO;2, 1998.

Huang, X., Olmez, I., Aras, N. K., and Gordon, G. E.: Emissions of trace elements from motor vehicles: Potential marker elements and source composition profile, Atmos. Environ., 28, 1385-1391, https://doi.org/10.1016/1352-2310(94)90201-1, 1994.

IPCC: Climate Change 2013: The Physical Science Basis, Cambridge University Press, Cambridge, UK and New York, NY, USA, 2013.

Kim, J.-H., Kim, S.-W., Ogren, J. A., Sheridan, P. J., Yoon, S.-C., Sharma, S., and Lin, N.-H.: Multiple scattering correction factor estimation for aethalometer aerosol absorption coefficient measurement, Aerosol Sci. Technol., 53, 160-171, https://doi.org/10.1080/02786826.2018.1555368, 2019.

Küpper, M., Quass, U., John, A. C., Kaminski, H., Leinert, S., Breuer, L., Gladtke, D., Weber, S., and Kuhlbusch, T. A. J.: Contributions of carbonaceous particles from fossil emissions and biomass burning to PM_{10} in the Ruhr area, Germany, Atmos. Environ., 189, 174-186, https://doi.org/10.1016/j.atmosenv.2018.06.039, 2018.

Lack, D. A., and Langridge, J. M.: On the attribution of black and brown carbon light absorption using the Ångström exponent, Atmos. Chem. Phys., 13, 10535-10543, https://doi.org/10.5194/acp-13-10535-2013, 2013.

Laskin, A., Laskin, J., and Nizkorodov, S. A.: Chemistry of atmospheric brown carbon, Chem. Rev., 115, 4335-4382, https://doi.org/10.1021/cr5006167, 2015.

Li, M., Zhang, Q., Kurokawa, J. I., Woo, J. H., He, K., Lu, Z., Ohara, T., Song, Y., Streets, D. G., Carmichael, G. R., Cheng, Y., Hong, C., Huo, H., Jiang, X., Kang, S., Liu, F., Su, H., and Zheng, B.: MIX: a mosaic Asian anthropogenic emission inventory under the international collaboration framework of the MICS-Asia and HTAP, Atmos. Chem. Phys., 17, 935-963, https://doi.org/10.5194/acp-17-935-2017, 2017.

Liakakou, E., Kaskaoutis, D. G., Grivas, G., Stavroulas, I., Tsagkaraki, M., Paraskevopoulou, D., Bougiatioti, A., Dumka, U. C., Gerasopoulos, E., and Mihalopoulos, N.: Long-term brown carbon

https://doi.org/10.5194/acp-2020-474
Preprint. Discussion started: 4 June 2020

spectral characteristics in a Mediterranean city (Athens), Sci. Total Environ., 708, 135019, https://doi.org/10.1016/j.scitotenv.2019.135019, 2020.

Lin, Y. C., Tsai, C. J., Wu, Y. C., Zhang, R., Chi, K. H., Huang, Y. T., Lin, S. H., and Hsu, S. C.: Characteristics of trace metals in traffic-derived particles in Hsuehshan Tunnel, Taiwan: size distribution, potential source, and fingerprinting metal ratio, Atmos. Chem. Phys., 15, 4117-4130, https://doi.org/10.5194/acp-15-4117-2015, 2015.

Liou, K. N.: An introduction to atmospheric radiation, (2nd ed.p 583), New York: Academic press, Elsevier Science, 2002.

Massabò, D., Caponi, L., Bernardoni, V., Bove, M. C., Brotto, P., Calzolai, G., Cassola, F., Chiari, M., Fedi, M. E., Fermo, P., Giannoni, M., Lucarelli, F., Nava, S., Piazzalunga, A., Valli, G., Vecchi, R., and Prati, P.: Multi-wavelength optical determination of black and brown carbon in atmospheric aerosols, Atmos. Environ., 108, 1-12, https://doi.org/10.1016/j.atmosenv.2015.02.058, 2015.

Moreno, T., Querol, X., Alastuey, A., de la Rosa, J., Sánchez de la Campa, A. M., Minguillón, M., Pandolfi, M., González-Castanedo, Y., Monfort, E., and Gibbons, W.: Variations in vanadium, nickel and lanthanoid element concentrations in urban air, Sci. Total Environ., 408, 4569-4579, https://doi.org/10.1016/j.scitotenv.2010.06.016, 2010.

Paatero, P., and Tapper, U.: Positive matrix factorization: A non-negative factor model with optimal utilization of error estimates of data values, Environmetrics, 5, 111-126, https://doi.org/10.1002/env.3170050203, 1994.

Pandey, A., Pervez, S., and Chakrabarty, R. K.: Filter-based measurements of UV–vis mass absorption cross sections of organic carbon aerosol from residential biomass combustion: Preliminary findings and sources of uncertainty, J. Quant. Spectrosc. Radiat. Transfer, 182, 296-304, https://doi.org/10.1016/j.jqsrt.2016.06.023, 2016.

Putaud, J. P., Van Dingenen, R., Alastuey, A., Bauer, H., Birmili, W., Cyrys, J., Flentje, H., Fuzzi, S., Gehrig, R., Hansson, H. C., Harrison, R. M., Herrmann, H., Hitzenberger, R., Hüglin, C., Jones, A. M., Kasper-Giebl, A., Kiss, G., Kousa, A., Kuhlbusch, T. A. J., Löschau, G., Maenhaut, W., Molnar, A., Moreno, T., Pekkanen, J., Perrino, C., Pitz, M., Puxbaum, H., Querol, X., Rodriguez, S., Salma, I., Schwarz, J., Smolik, J., Schneider, J., Spindler, G., ten Brink, H., Tursic, J., Viana, M.,

Wiedensohler, A., and Raes, F.: A European aerosol phenomenology – 3: Physical and chemical characteristics of particulate matter from 60 rural, urban, and kerbside sites across Europe, Atmos. Environ., 44, 1308-1320, https://doi.org/10.1016/j.atmosenv.2009.12.011, 2010.

Qin, Y. M., Tan, H. B., Li, Y. J., Li, Z. J., Schurman, M. I., Liu, L., Wu, C., and Chan, C. K.: Chemical characteristics of brown carbon in atmospheric particles at a suburban site near Guangzhou, China, Atmos. Chem. Phys., 18, 16409-16418, https://doi.org/10.5194/acp-18-16409-2018, 2018.

Qiu, C., Khalizov, A. F., Hogan, B., Petersen, E. L., and Zhang, R.: High sensitivity of diesel soot morphological and optical properties to combustion temperature in a shock tube, Environ. Sci. Technol., 48, https://doi.org/6444-6452, 10.1021/es405589d, 2014.

Ricchiazzi, P., Yang, S., Gautier, C., and Sowle, D.: SBDART: A Research and Teaching Software Tool for Plane-Parallel Radiative Transfer in the Earth's Atmosphere, Bull. Amer. Meteorol. Soc., 79, 2101-2114, https://doi.org/10.1175/1520-0477(1998)079<2101:SARATS>2.0.CO;2, 1998.

Sandradewi, J., Prévôt, A. S. H., Szidat, S., Perron, N., Alfarra, M. R., Lanz, V. A., Weingartner, E., and Baltensperger, U.: Using aerosol light absorption measurements for the quantitative determination of wood burning and traffic emission contributions to particulate matter, Environ. Sci. Technol., 42, 3316-3323, https://doi.org/10.1021/es702253m, 2008.

Sheesley, R. J., Schauer, J. J., Garshick, E., Laden, F., Smith, T. J., Blicharz, A. P., and Deminter, J. T.: Tracking personal exposure to particulate diesel exhaust in a diesel freight terminal using organic tracer analysis, J. Exposure Sci. Environ. Epidemiol., 19, 172-186, https://doi.org/10.1038/jes.2008.11, 2009.

Tao, J., Zhang, L., Cao, J., and Zhang, R.: A review of current knowledge concerning $PM_{2.5}$ chemical composition, aerosol optical properties and their relationships across China, Atmos. Chem. Phys., 17, 9485-9518, https://doi.org/10.5194/acp-17-9485-2017, 2017.

Tasoglou, A., Saliba, G., Subramanian, R., and Pandis, S. N.: Absorption of chemically aged biomass burning carbonaceous aerosol, J. Aerosol Sci., 113, 141-152, https://doi.org/10.1016/j.jaerosci.2017.07.011, 2017.

Tian, J., Wang, Q., Ni, H., Wang, M., Zhou, Y., Han, Y., Shen, Z., Pongpiachan, S., Zhang, N., Zhao, Z., Zhang, Q., Zhang, Y., Long, X., and Cao, J.: Emission characteristics of primary brown carbon

absorption from biomass and coal burning: Development of an optical emission inventory for China, J. Geophys. Res.-Atmos., 124, 1879-1893, https://doi.org/10.1029/2018JD029352, 2019.

Tian, J., Wang, Q., Han, Y., Ye, J., Wang, P., Pongpiachan, S., Ni, H., Zhou, Y., Wang, M., Zhao, Y., and Cao, J.: Contributions of aerosol composition and sources to particulate optical properties in a southern coastal city of China, Atmos. Res., 235, 104744, https://doi.org/10.1016/j.atmosres.2019.104744, 2020.

Wang, J., Ho, S. S. H., Ma, S., Cao, J., Dai, W., Liu, S., Shen, Z., Huang, R., Wang, G., and Han, Y.: Characterization of $PM_{2.5}$ in Guangzhou, China: uses of organic markers for supporting source apportionment, Sci. Total Environ., 550, 961-971, https://doi.org/10.1016/j.scitotenv.2016.01.138, 2016.

Wang, J., Nie, W., Cheng, Y., Shen, Y., Chi, X., Wang, J., Huang, X., Xie, Y., Sun, P., Xu, Z., Qi, X., Su, H., and Ding, A.: Light absorption of brown carbon in eastern China based on 3-year multi-wavelength aerosol optical property observations and an improved absorption Ångström exponent segregation method, Atmos. Chem. Phys., 18, 9061-9074, https://doi.org/10.5194/acp-18-9061-2018, 2018.

Wang, L., Li, Z., Tian, Q., Ma, Y., Zhang, F., Zhang, Y., Li, D., Li, K., and Li, L.: Estimate of aerosol absorbing components of black carbon, brown carbon, and dust from ground-based remote sensing data of sun-sky radiometers, J. Geophys. Res.-Atmos., 118, 6534-6543, https://doi.org/10.1002/jgrd.50356, 2013.

Wang, Q., Cao, J., Han, Y., Tian, J., Zhu, C., Zhang, Y., Zhang, N., Shen, Z., Ni, H., Zhao, S., and Wu, J.: Sources and physicochemical characteristics of black carbon aerosol from the southeastern Tibetan Plateau: internal mixing enhances light absorption, Atmos. Chem. Phys., 18, 4639-4656, https://doi.org/10.5194/acp-18-4639-2018, 2018a.

Wang, Q. Y., Cao, J. J., Han, Y. M., Tian, J., Zhang, Y., Pongpiachan, S., Zhang, Y. G., Li, L., Niu, X. Y., Shen, Z. X., Zhao, Z. Z., Tipmanee, D., Bunsomboonsakul, S., Chen, Y., and Sun, J.: Enhanced light absorption due to the mixing state of black carbon in fresh biomass burning emissions, Atmos. Environ., 180, 184-191, https://doi.org/10.1016/j.atmosenv.2018.02.049, 2018b.

Wang, Q., Han, Y., Ye, J., Liu, S., Pongpiachan, S., Zhang, N., Han, Y., Tian, J., Wu, C., Long, X., Zhang, Q., Zhang, W., Zhao, Z., and Cao, J.: High Contribution of Secondary Brown Carbon to Aerosol Light Absorption in the Southeastern Margin of Tibetan Plateau, Geophys. Res. Lett., 46, 4962-4970, https://doi.org/10.1029/2019GL082731, 2019a.

Wang, Q., Ye, J., Wang, Y., Zhang, T., Ran, W., Wu, Y., Tian, J., Li, L., Zhou, Y., Hang Ho, S. S., Dang, B., Zhang, Q., Zhang, R., Chen, Y., Zhu, C., and Cao, J.: Wintertime Optical Properties of Primary and Secondary Brown Carbon at a Regional Site in the North China Plain, Environ. Sci. Technol., 53, 12389-12397, 10.1021/acs.est.9b03406, 2019b.

Wang, Y. Q., Zhang, X. Y., and Draxler, R. R.: TrajStat: GIS-based software that uses various trajectory statistical analysis methods to identify potential sources from long-term air pollution measurement data, Environ. Modell. Softw., 24, 938-939, https://doi.org/10.1016/j.envsoft.2009.01.004, 2009.

Xie, M., Hays, M. D., and Holder, A. L.: Light-absorbing organic carbon from prescribed and laboratory biomass burning and gasoline vehicle emissions, Sci. Rep., 7, https://doi.org/10.1038/s41598-017-06981-8, 2017.

Xing, J., Shao, L., Zhang, W., Peng, J., Wang, W., Shuai, S., Hu, M., and Zhang, D.: Morphology and size of the particles emitted from a gasoline-direct-injection-engine vehicle and their ageing in an environmental chamber, Atmos. Chem. Phys., 20, 2781-2794, https://doi.org/10.5194/acp-20-2781-2020, 2020.

Xu, H. M., Cao, J. J., Ho, K. F., Ding, H., Han, Y. M., Wang, G. H., Chow, J. C., Watson, J. G., Khol, S. D., Qiang, J., and Li, W. T.: Lead concentrations in fine particulate matter after the phasing out of leaded gasoline in Xi'an, China, Atmos. Environ., 46, 217-224, https://doi.org/10.1016/j.atmosenv.2011.09.078, 2012.

Yang, M., Howell, S. G., Zhuang, J., and Huebert, B. J.: Attribution of aerosol light absorption to black carbon, brown carbon, and dust in China – interpretations of atmospheric measurements during EAST-AIRE, Atmos. Chem. Phys., 9, 2035-2050, https://doi.org/10.5194/acp-9-2035-2009, 2009.

Zanatta, M., Gysel, M., Bukowiecki, N., Müller, T., Weingartner, E., Areskoug, H., Fiebig, M., Yttri, K. E., Mihalopoulos, N., Kouvarakis, G., Beddows, D., Harrison, R. M., Cavalli, F., Putaud, J. P., Spindler, G., Wiedensohler, A., Alastuey, A., Pandolfi, M., Sellegri, K., Swietlicki, E., Jaffrezo, J.

L., Baltensperger, U., and Laj, P.: A European aerosol phenomenology-5: Climatology of black carbon optical properties at 9 regional background sites across Europe, Atmos. Environ., 145, 346-364, https://doi.org/10.1016/j.atmosenv.2016.09.035, 2016.

Zhang, T., Cao, J. J., Tie, X. X., Shen, Z. X., Liu, S. X., Ding, H., Han, Y. M., Wang, G. H., Ho, K. F., Qiang, J., and Li, W. T.: Water-soluble ions in atmospheric aerosols measured in Xi'an, China: Seasonal variations and sources, Atmos. Res., 102, 110-119, https://doi.org/10.1016/j.atmosres.2011.06.014, 2011.

Zhao, Z., Cao, J., Chow, J. C., Watson, J. G., Chen, A. L. W., Wang, X., Wang, Q., Tian, J., Shen, Z., Zhu, C., Liu, S., Tao, J., Ye, Z., Zhang, T., Zhou, J., and Tian, R.: Multi-wavelength light absorption of black and brown carbon at a high-altitude site on the Southeastern margin of the Tibetan Plateau, China, Atmos. Environ., 212, 54-64, https://doi.org/10.1016/j.atmosenv.2019.05.035, 2019.

Zheng, H., Kong, S., Wu, F., Cheng, Y., Niu, Z., Zheng, S., Yang, G., Yao, L., Yan, Q., Wu, J., Zheng, M., Chen, N., Xu, K., Yan, Y., Liu, D., Zhao, D., Zhao, T., Bai, Y., Li, S., and Qi, S.: Intra-regional transport of black carbon between the south edge of the North China Plain and central China during winter haze episodes, Atmos. Chem. Phys., 19, 4499-4516, https://doi.org/10.5194/acp-19-4499-2019, 2019.

Zhong, M., and Jang, M.: Dynamic light absorption of biomass-burning organic carbon photochemically aged under natural sunlight, Atmos. Chem. Phys., 14, 1517-1525, https://doi.org/10.5194/acp-14-1517-2014, 2014.

Zhu, C.-S., Cao, J.-J., Hu, T.-F., Shen, Z.-X., Tie, X.-X., Huang, H., Wang, Q.-Y., Huang, R.-J., Zhao, Z.-Z., Močnik, G., and Hansen, A. D. A.: Spectral dependence of aerosol light absorption at an urban and a remote site over the Tibetan Plateau, Sci. Total Environ., 590-591, 14-21, https://doi.org/10.1016/j.scitotenv.2017.03.057, 2017.

Zotter, P., Herich, H., Gysel, M., El-Haddad, I., Zhang, Y., Močnik, G., Hüglin, C., Baltensperger, U., Szidat, S., and Prévôt, A. S. H.: Evaluation of the absorption Ångström exponents for traffic and wood burning in the Aethalometer-based source apportionment using radiocarbon measurements of ambient aerosol, Atmos. Chem. Phys., 17, 4229-4249, https://doi.org/10.5194/acp-17-4229-2017, 2017.

https://doi.org/10.5194/acp-2020-474
Preprint. Discussion started: 4 June 2020

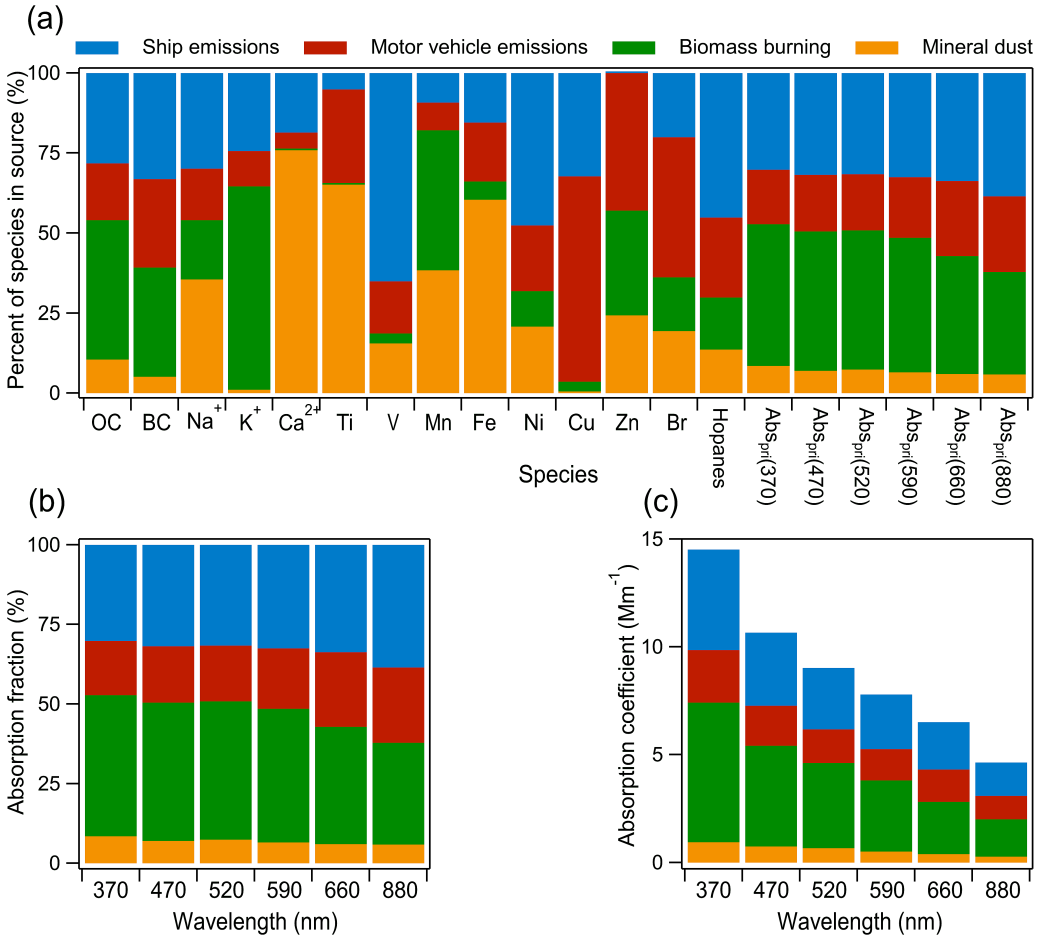

Figure 1. (a) Source profiles for the four sources identified by the positive matrix factorization model, (b) the contribution of each source to primary aerosol light absorption, and (c) the primary aerosol light absorption coefficients of each source at different wavelengths during the campaign.

https://doi.org/10.5194/acp-2020-474
Preprint. Discussion started: 4 June 2020

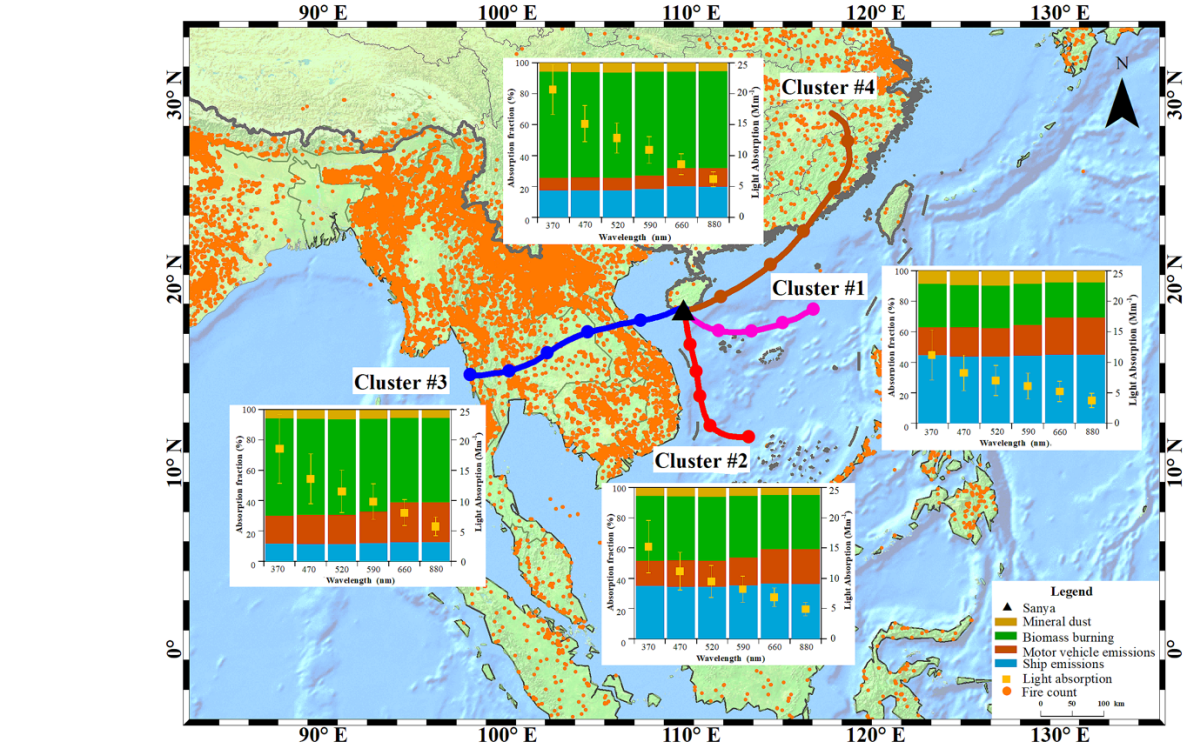

Figure 2. Contribution of each source to primary aerosol light absorption at each three-day backward-trajectory cluster during the campaign at Sanya. The map was drawn using ArcGIS software. The base map is the World Topographic Map from © ESRI (Environmental Systems Research Institute, Inc.) (www.arcgis.com/home/item.html?id=30e5fe3149c34df1ba922e6f5bbf808f).

https://doi.org/10.5194/acp-2020-474
Preprint. Discussion started: 4 June 2020

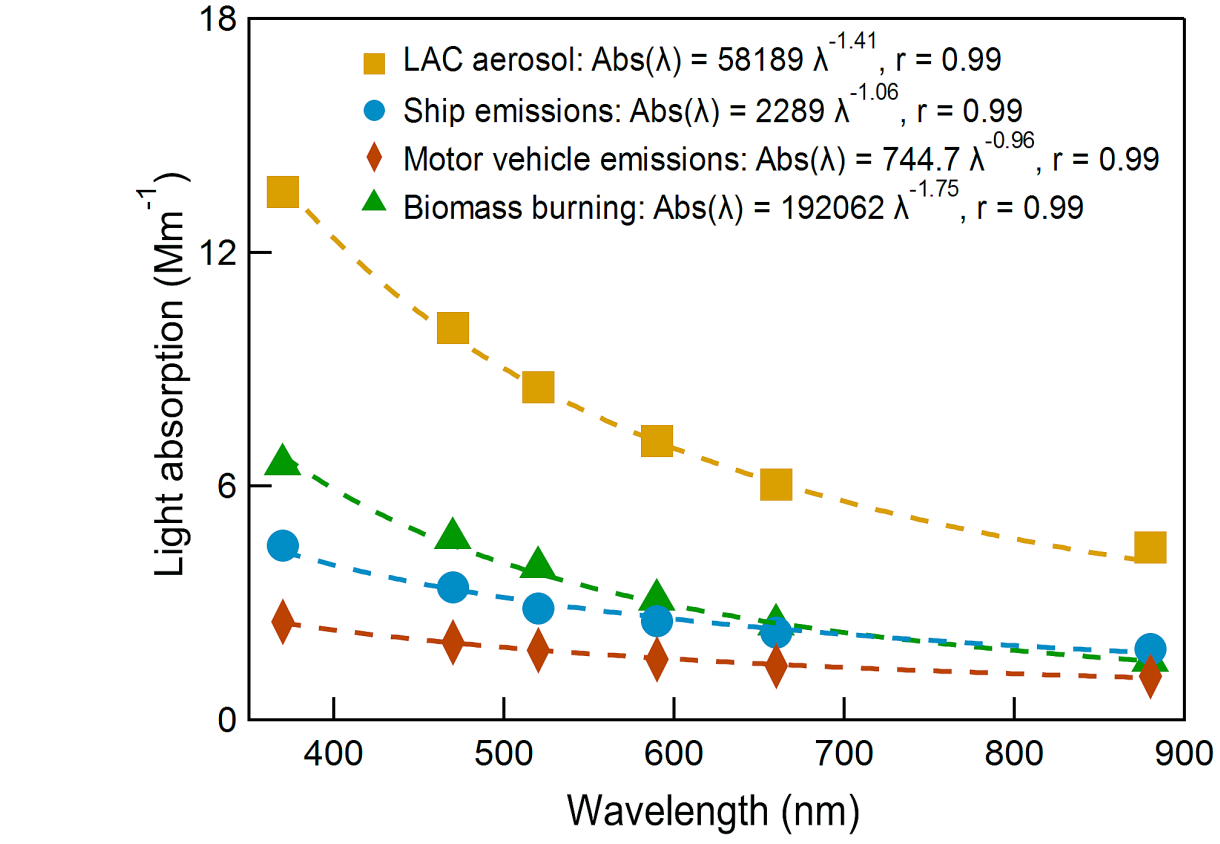

Figure 3. The distributions of light absorption (Abs(λ)) of total light-absorbing carbonaceous (LAC) aerosol and those from ship emissions, traffic emissions, and biomass burning. The dash line is power law fit.

https://doi.org/10.5194/acp-2020-474
Preprint. Discussion started: 4 June 2020

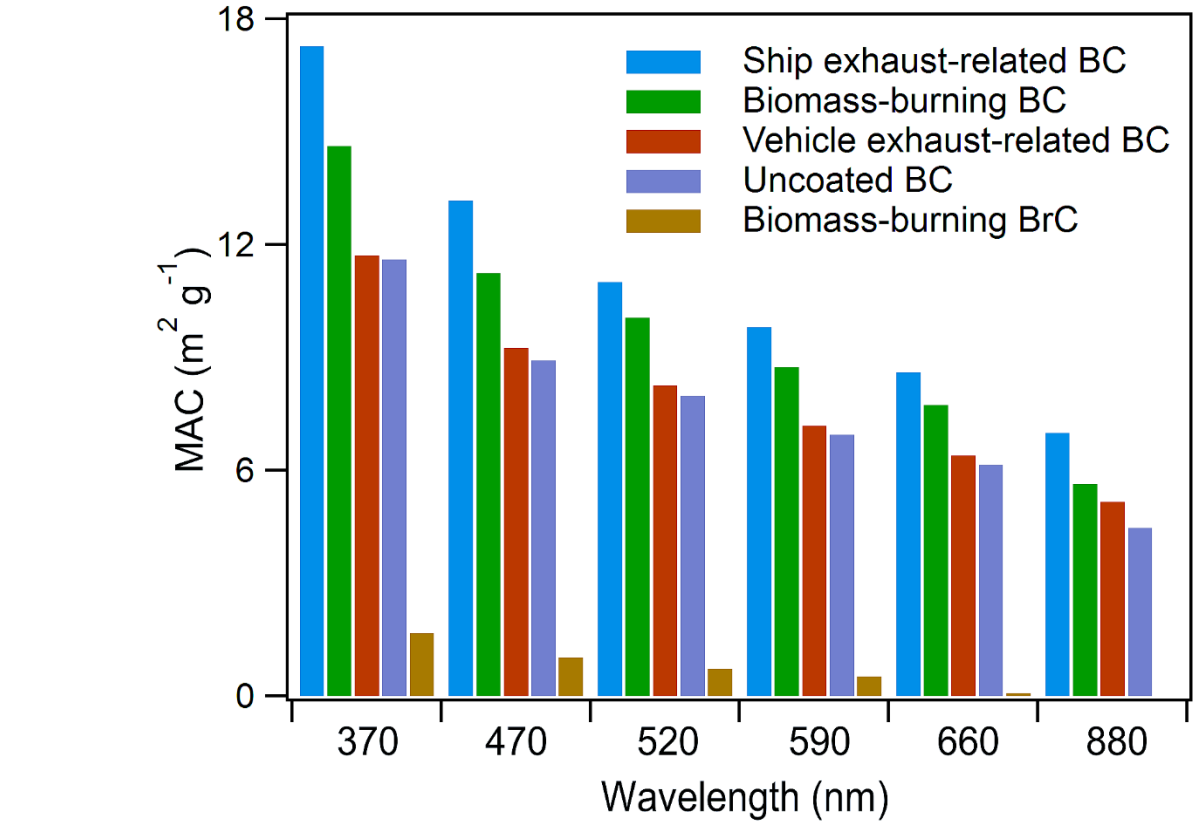

Figure 4. The source-specific mass absorption cross section (MAC) of black carbon (BC) and brown carbon (BrC) at different wavelengths. The MAC of uncoated BC particles at each wavelength are extrapolated from 7.5 m^2 g^{-1} at 550 nm (Bond and Bergstrom, 2006) by assuming an BC absorption Ångström exponent of 1.1.

https://doi.org/10.5194/acp-2020-474
Preprint. Discussion started: 4 June 2020

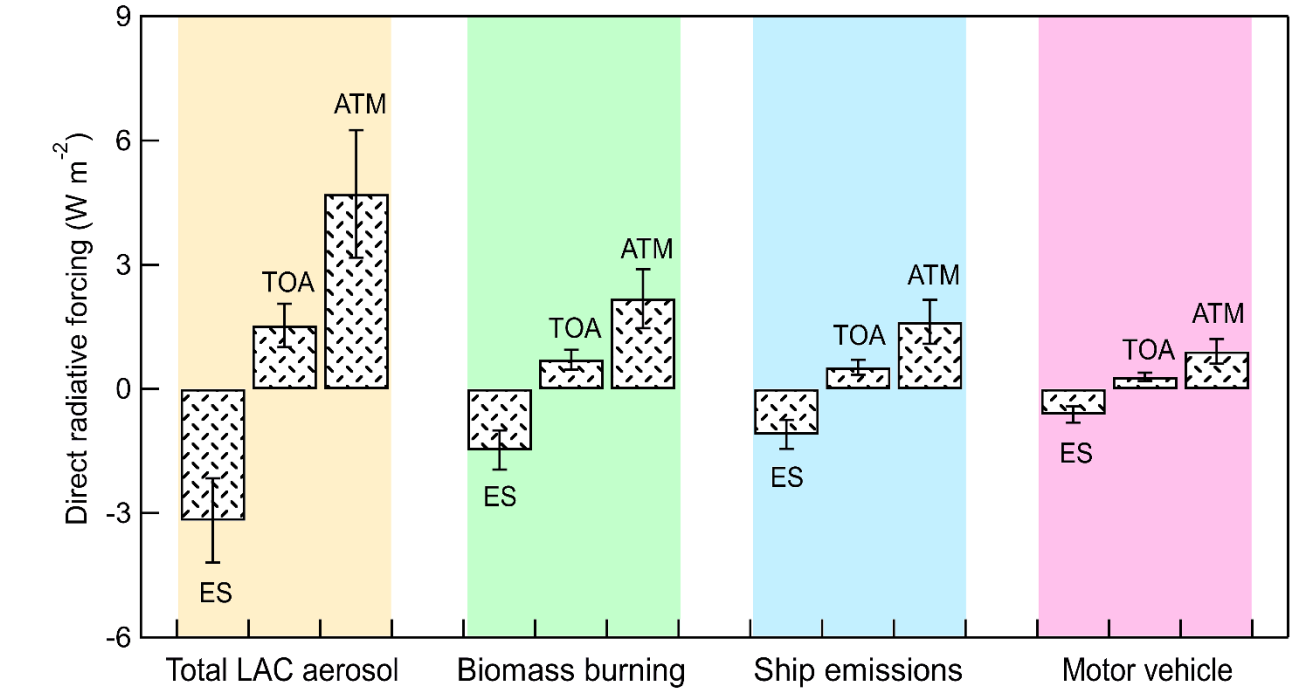

Figure 5. Distributions of direct radiative forcing (DRF) caused by light-absorbing carbonaceous aerosol from biomass burning, ship emissions, and motor vehicle emissions. The error bar represents one standard deviation. ES, TOA, ATM represent the DRF at the Earth's surface, the top of the atmosphere, and in the atmosphere, respectively.